

# Real-Time Intracellular Transport of Gene Nanocarriers Studied by Multiple Particle Tracking

Junghae Suh,<sup>†</sup> Denis Wirtz,<sup>‡</sup> and Justin Hanes<sup>\*,†,‡</sup>

Department of Biomedical Engineering, The Johns Hopkins University, 720 Rutland Ave., Baltimore, Maryland 21205, and Department of Chemical & Biomolecular Engineering, The Johns Hopkins University, 3400 N. Charles St., Baltimore, Maryland 21218

We used real-time multiple particle tracking to quantitatively characterize the type and rates of transport of gene nanocarriers within live cells. The heterogeneous cytoplasmic transport of polyethylenimine (PEI)/DNA gene carriers was quantified by tracking their mean-square displacements over time and classified into active and nonactive transport populations on the basis of their effective diffusivities versus time. Nonactive gene carriers frequently displayed hop-diffusion trajectories, suggesting a porous cytoplasmic network of flexible biopolymers or sequential attachment and detachment events. Microtubule-dependent active transport of gene carriers resulted in an effective diffusivity 30-fold greater than that of nonactive carriers (at a time scale of 3 s). Compared to nonactive carriers in control cells with intact microtubules, microtubule depolymerization enhanced short-range motion of gene carriers but resulted in similar long-range transport. Multiple particle tracking characterizes gene carrier transport in complex biological environments and, therefore, may be a useful tool in quantifying rate-limiting steps in gene delivery within cells and other biological media.

## Introduction

Gene delivery is a complex process with many possible rate-limiting steps. Potential bottlenecks to intracellular gene delivery with nonviral systems include (1, 2) cell uptake, endosome escape, nuclear uptake, and vector unpacking. The cytoplasmic transport of nonviral gene carriers has received relatively little quantitative attention. After cellular uptake by endocytosis, gene carriers must traverse the expansive and molecularly crowded cytoplasm to reach the nucleus. However, the biophysical and biological mechanisms underlying cytoplasmic transport of gene carriers are poorly characterized.

Quantitative studies on the diffusion of particulates, including gene carriers, in the cytoplasm have been sparse since investigations of dynamic processes are not possible with static methods such as electron microscopy or fixed-cell confocal microscopy. Studies of the diffusion of DNA fragments in cells using fluorescence recovery after photobleaching (FRAP) have demonstrated that the cytoplasm may be a critical barrier to nuclear gene delivery (3). Gene carrier transport to the perinuclear region of the cell is poorly characterized (4, 5) but is believed to involve movement through endosomes (6, 7) and diffusion of vectors (5). Co-localization with lysosomal markers has shown that some gene carriers are routed to lysosomes to be degraded, whereas others are not (8). PEI and polylysine are both cationic polymers with the ability to condense DNA; however, they traffic to different intracellular destinations (8) and result in different transfection efficiencies (9). The involvement of cytoskeletal elements in the intracellular transport of gene

carriers is probable (10), especially because transport of endosomes requires such structures. Importantly, the mechanism by which a DNA vector is trafficked intracellularly may have important implications on the efficiency of gene delivery. If vectors are trafficked to sites far from the nucleus, for example, gene delivery may be hindered by the crowded cytoplasm. Thus, our research aims to identify and quantify, both temporally and spatially, the intracellular transport properties of gene nanocarriers in real time.

Particle tracking technology, albeit typically of single particles, has been used to study a variety of biological phenomena, such as the movements of lipid molecules (11) and proteins embedded (12) in the plasma membrane of cells. Subsequently, multiple particle tracking has been developed to ascertain the local viscoelastic properties of complex environments, such as actin networks (13) and the cell cytoplasm (14). We have recently developed live-cell multiple particle tracking (MPT) to quantitatively characterize the transport of nonviral gene carriers in live cells (10). By coupling fluorescence microscopy with MPT, spatiotemporal information such as rates of individual particle movements (e.g., diffusivity and velocity), the mode of transport (e.g., random versus directed or active), and the trajectory and directionality of the transport can be quantified with 33 ms and ~5 nm resolution (13). Understanding the quantitative and qualitative transport properties of gene carriers may determine limitations of current vectors and identify strategies for improvement.

Recent studies from our group utilizing MPT have shed light on the cytoplasmic transport of nonviral PEI/DNA gene carriers in live cells (10). PEI/DNA nanocomplexes utilize microtubules for rapid, active transport to the perinuclear region in COS-7 cells (10), perhaps partially

\* To whom correspondence should be addressed. Phone: (410) 516-3484. Email: hanes@jhu.edu.

<sup>†</sup> Department of Biomedical Engineering.

<sup>‡</sup> Department of Chemical & Biomolecular Engineering.

explaining why these carriers are among the most efficient vehicles for gene transfection.

Here, we present our continuing efforts to quantitatively characterize the cytoplasmic transport of PEI/DNA gene carriers using MPT. Specifically, we discuss in greater detail how intracellular PEI/DNA nanocomplexes display a nonnormal distribution of transport rates that can be quantitatively and qualitatively characterized into active and nonactive populations. More in-depth analysis is presented on carriers described as diffusive and subdiffusive (10). Last, rates of nonactively transported gene carriers in microtubule-depolymerized cells are more closely examined to obtain greater insight on microtubule-dependent gene carrier transport.

## Experimental Procedures

### Fluorescent Labeling of PEI and PEI Complexes.

Polyethylenimine (PEI) (25 kDa MW, branched, Sigma) was labeled with Oregon Green 514 (Molecular Probes) according to manufacturer's protocol with reaction time extended to 2 h. PEI was added to salmon DNA (Sigma), both in 150 mM NaCl, for complexes of N/P (nitrogen-to-phosphate ratio) equal to 6. The mixture was quickly vortexed, and complexes were allowed to form for 30 min at room temperature.

Our current studies track the PEI label of PEI/DNA complexes. With dual-labeling confocal microscopy studies, Bieber and co-workers have shown that DNA remains associated with PEI even at 18 h post-transfection (15).

Additionally, modifying PEI with the fluorescent dye Oregon Green is likely to alter the physicochemical properties of the PEI/DNA complexes. Complexes formed with labeled PEI were verified to transfect COS-7 cells, although at 3-fold lower efficiencies (data not shown).

Complexes in this study are formed with salmon DNA, which are approximately 2 kb (Sigma); however, plasmid DNA commonly used for transfection may be 2–3 times that size. The PEI/DNA complexes used in this study have a number average diameter of 138.3 nm and an average  $\zeta$  potential of 13.8 mV, both measured with a Malvern Zetasizer 3000 (Southborough, MA), values which are similar to complexes made with unlabeled PEI and plasmid DNA (data not shown).

**Cells.** COS-7 cells, plated onto glass-bottom tissue culture plates (MatTek Corp.), were arrested in the G<sub>0</sub>/G<sub>1</sub> cell cycle stage by serum deprivation (10). The propidium iodide cell cycle assay (16) indicated this method resulted in 80–85% of cells being in G<sub>0</sub>/G<sub>1</sub> in 48 h. To transfect cells, gene carriers were added directly to the media. Cells were then washed with Hank's Buffered Salt Solution, and fresh media was added 1 h post-transfection. To depolymerize microtubules, cells were treated with 10  $\mu$ M nocodazole 1 h prior to transfection.

**Fluorescence Microscopy and Real-Time Particle Tracking.** Cells were observed under an epifluorescence microscope (Nikon Inc.) equipped with a 100X magnification, 1.3 numerical aperture oil-immersion lens (Nikon Inc.) at 37 °C; 20-s time lapses were recorded with a SIT camera (Dage-MTI) at 30 frames/s (13). A CCD camera (Hamamatsu) was used to capture phase contrast images of the cells. All movies were analyzed with MetaMorph software (Universal Imaging Corp.) to extract  $x$  and  $y$  positional data of gene carriers over time. The spatial resolution, which was evaluated by tracking the apparent displacement of latex beads immobilized on the coverslip, was  $\sim$ 5 nm (13). Nanometer resolution is obtained on the displacements of multiple particles simultaneously by tracking the light-intensity-weighted centroid of diffrac-

tion-limited images, thereby achieving resolutions much higher than a pixel (13, 17). Mean-square displacement (MSD) in two dimensions,  $x$  and  $y$ , is given by

$$\langle \Delta r^2(\tau) \rangle = \langle \Delta x^2 + \Delta y^2 \rangle \quad (1)$$

We assume the cytoplasm is isotropic, and thus particle displacements in the  $x$ ,  $y$ , and  $z$ -axes are uncorrelated. Therefore,  $\text{MSD}_{2D} = \langle \Delta x^2 \rangle + \langle \Delta y^2 \rangle = 2/3 \text{MSD}_{3D} = 2/3[\langle \Delta x^2 \rangle + \langle \Delta y^2 \rangle + \langle \Delta z^2 \rangle]$ . For a general case of particle transport in 2-D,  $\langle \Delta r^2(\tau) \rangle$  (or MSD) is equal to

$$\langle \Delta r^2(\tau) \rangle = 4D_{\text{eff}}(\tau)\tau \quad (2)$$

where  $D_{\text{eff}}(\tau)$  is the effective diffusion coefficient and  $\tau$  is the time scale. Using the MSD value at various time scales ( $\tau$ ), we are able to calculate the  $D_{\text{eff}}$  of gene carriers as a function of time.

**Transport Mode Categorization.** Particles undergoing simple diffusion display an effective diffusivity ( $D_{\text{eff}}$ ) that is constant with time scale ( $\tau$ ) and, therefore, fits the Stokes–Einstein relation,  $D = k_B T / 6\pi\eta a$ , where  $k_B$  is Boltzmann's constant,  $T$  is temperature in Kelvin,  $\eta$  is viscosity, and  $a$  is particle radius. Particles with  $D_{\text{eff}}(\tau)$  decreasing with  $\tau$  are categorized as subdiffusive, and those with increasing  $D_{\text{eff}}(\tau)$  over  $\tau$  are termed actively transported. The movement of actively transported complexes are described by

$$\langle \Delta r^2(\tau) \rangle = 4D\tau + v^2\tau^2 \quad (3)$$

where the added term characterizes particle transport due to directed motion, with  $D$  as the diffusion coefficient and  $v$  as the mean nanocomplex velocity.

## Results and Discussion

**Gene Carrier Transport Rates.** To characterize the intracellular transport barrier to gene delivery, we used multiple particle tracking (MPT) to study the transport of nonviral PEI/DNA nanocomplexes. Gene carriers were formed by spontaneous assembly following the mixing of aqueous solutions of branched PEI (25 kDa) and linear salmon DNA. After formation, carriers were added to cells arrested in the G<sub>0</sub>/G<sub>1</sub> phase of the cell cycle (i.e., nondividing cells), and their transport was tracked by high-resolution video microscopy.

Trajectories of gene carriers within COS-7 cells, examples of which are shown in Figure 1A, are heterogeneous in character. It is striking that many carriers appear nearly immobile during the 20 s of observation, whereas others move rapidly and cover large distances.

The transport of intracellular PEI/DNA nanocomplexes was quantified by plotting their mean-square displacements (MSD) as a function of time,  $\tau$ , as shown in Figure 1B. Particles moving by pure diffusion have a slope of 1 on a log–log plot since  $\text{MSD} \sim \tau$  for this case. A non-Gaussian distribution of MSDs is evident at various time scales (Figure 1C shows time scale of 3 s), supporting the visual observation that intracellular nanocomplexes are transported at nonuniform rates and that some carriers move significantly faster (by several orders of magnitude at the longer time scales) than others.

The distribution of effective diffusivities for individual particles (Figure 1D) shows most gene carriers exhibit effective diffusivities that are less than half of the average  $D_{\text{eff}}$ , but several outlying gene carriers display  $D_{\text{eff}}$  manyfold greater than the average (see inset of Figure 1D). The broad range of diffusivity values confirms the qualitative observation that gene carriers are trans-

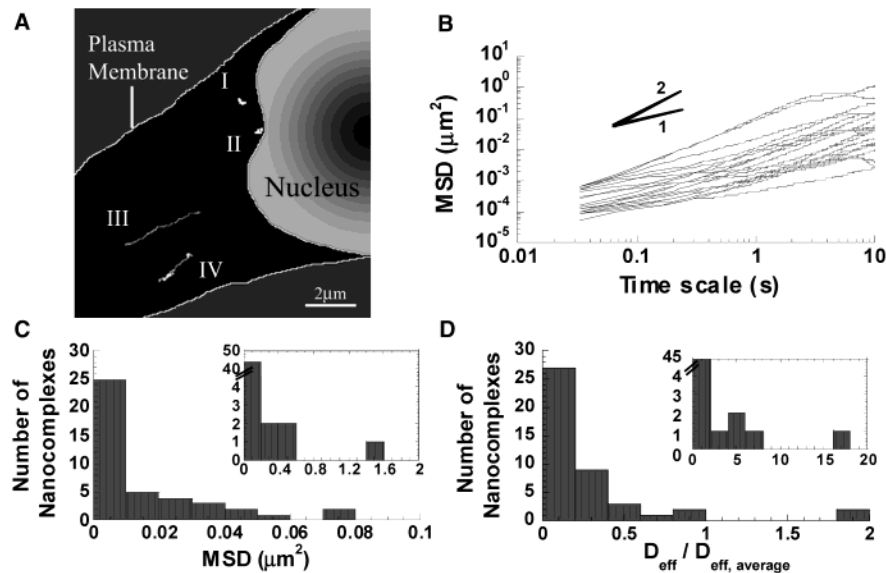


**Figure 1.** (A) Four example trajectories (I–IV) of PEI/DNA nanocomplexes within a single COS-7 cell. (B) Mean-square displacements (MSD) of intracellular PEI/DNA nanocomplexes in COS-7 cells 2 h post-transfection (data for 20 nanocomplexes shown). (C) Distribution of MSD (time scale,  $\tau$ , of 3 s) of nanocomplexes ( $n = 49$ ) at 2 h post-transfection. (D) Effective diffusivities ( $D_{\text{eff}}$ ) of nanocomplexes ( $n = 49$ ) normalized to the average effective diffusivity ( $D_{\text{eff,av}}$ ) at 2 h post-transfection using a time scale,  $\tau$ , of 3 s.

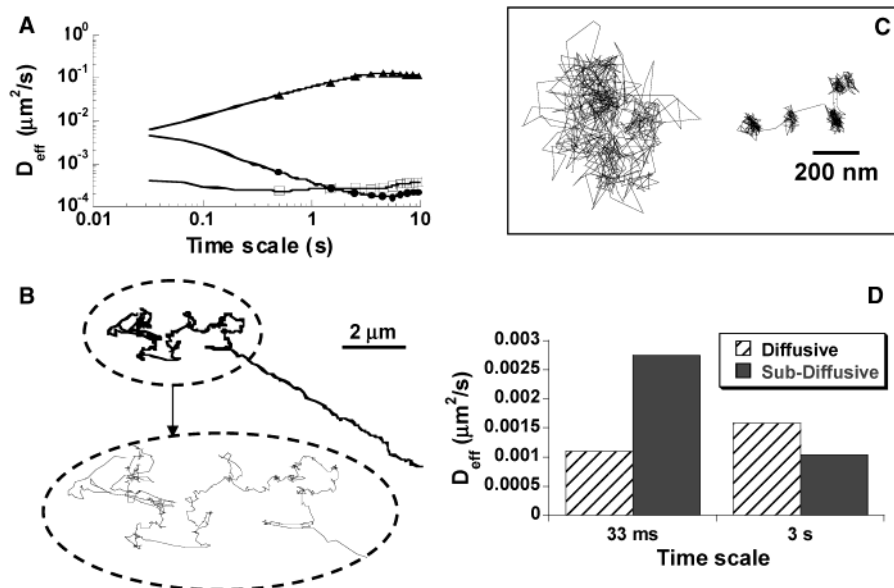


**Figure 2.** (A) Transport modes of gene carriers are classified into three groups based on their characteristic  $D_{\text{eff}}$  curves: diffusive ( $\square$ ), subdiffusive ( $\bullet$ ), and active ( $\blacktriangle$ ). The markers of only 10 data points per gene carrier are shown to distinguish the curves. (B) Twenty-second trajectory of an actively transported gene carrier. Periods of saltatory (stop and go) motion can be seen in the expanded oval. (C) Example trajectories of subdiffusive or diffusive gene carriers. (D)  $D_{\text{eff}}$  of diffusive and subdiffusive gene carriers at short (33 ms) and long (3 s) time scales. Kruskal–Wallis test determined the  $D_{\text{eff}}$ 's for diffusive carriers are similar at the two time scales, whereas the difference between  $D_{\text{eff}}$ 's for subdiffusive carriers are statistically significant ( $p < 10^{-5}$ ) at the two different time scales.

ported nonuniformly over the same time course. Importantly, the distribution of transport rates (e.g., over 3 orders of magnitude in MSD at a time scale of 10 s) cannot be explained by differences in diffusivities of individual particles (in accordance with the Stokes–Einstein relation). First, the gene carriers do not span 3 orders of magnitude in size. In addition, most carriers do not even move by simple diffusion, as determined by the fact that the slopes of individual particle MSD curves rarely increase as  $\tau^{-1}$  (or have a slope of 1 on a log–log plot). Indeed, the heterogeneous environment within a cell, with a mean cytoplasmic mesh radius of  $\sim 50$  nm (18) that is created by cellular components (such as microtubules, actin, and intermediate filaments), is not likely to support purely Brownian transport of colloids that have sizes on the order of 100–200 nm.

Whether a correlation exists between gene carrier transport rate and gene delivery success by that carrier is unclear. For example, a fast-moving gene carrier may be more successful at delivering genes because it can traverse the cytoplasm and reach the nucleus the fastest. However, since PEI/DNA nanocomplexes are likely to be transported within vesicles along the endolysosomal pathway (6, 10); it is possible that the range of  $D_{\text{eff}}$  observed here is a reflection of the transport rates of the vesicles (e.g., early endosomes, late endosomes, lysosomes) in which the gene carriers are (transiently) trapped. In other words, the transport rate of the gene carrier may change as the carrier is transferred progressively from the plasma membrane to the perinuclear region.

**Modes of Intracellular Transport.** A strength of MPT is that the intracellular transport of gene carriers

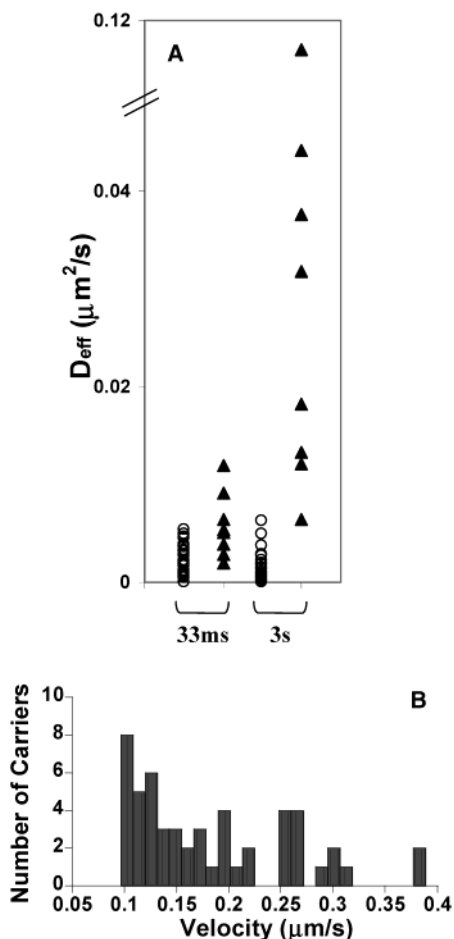


**Figure 3.** (A) Effective diffusivities of active (▲) and nonactive (○) PEI/DNA nanocomplexes at short ( $\tau = 33$  ms) and long ( $\tau = 3$  s) time scale at 2 h post-transfection. (B) Distribution of velocities of actively transported PEI nanocomplexes in COS-7 cells.

can be categorized into three groups on the basis of their characteristic  $D_{\text{eff}}$  curves: diffusive, subdiffusive, or active (Figure 2A). A purely diffusive gene carrier has a constant  $D_{\text{eff}}$  over time. If the carrier's  $D_{\text{eff}}$  decreases with time scale, they are classified as subdiffusive, and actively transported carriers have  $D_{\text{eff}}$  that increase with time scale. The percentage of gene carriers exhibiting each type of transport mode over various times post-transfection are presented elsewhere (10).

Actively transported carriers often exhibit a period of saltatory (stop and go) motion, as well as a processively linear/curvilinear path (Figure 2B), a property potentially attributable to motor protein-mediated active transport. Diffusive and subdiffusive carriers each display two types of trajectories. One is an apparently random motion (left of Figure 2C), and the other may be described as hop diffusion (right of Figure 2C). Kusumi et al. observed phospholipids exhibiting hop diffusion in the compartmentalized membrane of cells (19).

"Diffusive" carriers that exhibit hop diffusion are unlikely to be moving in a purely viscous medium. These carriers fit our criteria of "diffusive" in that their  $D_{\text{eff}}$  is constant with time scale over (Figure 2D) the entire probed time (33 ms to 10 s) (Figure 2A). Future classifications should take into account not only the shape of the  $D_{\text{eff}}$  curves (i.e.,  $D_{\text{eff}} \sim \tau^0$ ) (Figure 2A), but also the pattern of the trajectories (i.e., not hop diffusion) (Figure 2C).

A possible explanation for the observed hop diffusion of some of the gene carriers (Figure 2C) is that these

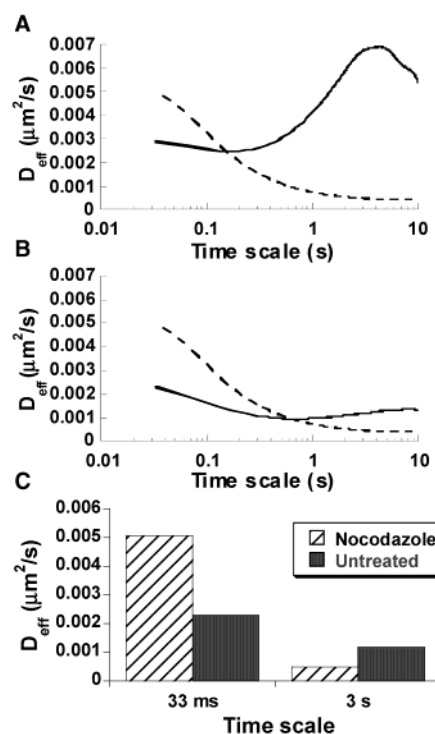


**Figure 4.** (A) Effective diffusivities,  $D_{\text{eff}}$ , of PEI nanocomplexes in untreated (solid) and nocodazole-treated (dotted) cells at 2 h post-transfection. (B) Same as in A, except for the untreated case (control), the contributions of actively transported gene carriers are omitted. (C)  $D_{\text{eff}}$ , at short (33ms) and long (3s) time scales, of gene carriers in nocodazole-treated and control cells where the contributions of actively transported gene carriers are omitted. The difference in  $D_{\text{eff}}$ 's between nocodazole-treated and control cells is statistically significant ( $p < 10^{-4}$ ) for the short time scale (33 ms) but not for the long time scale (3 s), as determined by the Kruskal–Wallis test.

carriers are traversing a molecularly crowded yet porous network (formed by various cytoskeletal elements or organelles) within cells. The gene carrier may be tightly caged by cytoskeletal elements, requiring relaxation of cytoskeletal polymers before the gene carrier can move to its next caged environment. Alternatively, the "pearls-on-a-string" trajectory may be caused by alternate gene carrier binding to subcellular structures followed by detachment and binding to another intracellular structure. For either hypothesis, gene carriers can be inside or outside of intracellular vesicles.

From this point in the paper, we will discuss active versus nonactive transport modes where the nonactively transported carriers display restricted and/or hop diffusion (i.e., combination of diffusive and subdiffusive categories). At 2 h post-transfection, the majority (84%) of gene carriers are found to be nonactively transported (10).

**Actively Transported Gene Carriers.** To compare the transport properties of actively transported versus nonactively transported gene carriers, we calculated the effective diffusivities of the two groups at two time scales (Figure 3A). Values of  $D_{\text{eff}}$  at the short time scale of 33 ms reveal that the short-range motion of the active and nonactive carriers is similar. At this short time scale, the  $D_{\text{eff}}$  values of actively transported carriers are minimally affected by convection and  $D_{\text{eff}} = D$  (eq 3). The random diffusion component of actively transported carriers ( $4D\tau$  of eq 3) being similar to the random diffusion of nonactive carriers at this short time scale implies that both types of carriers experience comparable microenvironments. At a longer time scale of 3 s, however, actively transported carriers have an average  $D_{\text{eff}}$  that is 30-fold greater than

nonactive carriers. Thus, even though both active and nonactive gene carriers move similarly for short times, actively transported gene carriers eventually travel subcellular distances much greater than that of nonactive carriers. It is possible that nonactive carriers may become active at a different time, particularly if a nonactive carrier is within an early endosome tethered to the cytoskeleton. The early endosome may then be actively transported along microtubules by motor proteins to other intracellular processing sites, such as lysosomes.

We extracted the average velocity of each actively transported carrier from their MSDs by realizing that, at longer time scales, MSD is dominated by the term  $v^2t^2$  (from eq 3) with  $v$  as velocity. The velocities of actively transported carriers (Figure 3B) are of the same order of magnitude as that previously reported for motor protein-mediated transport (20). Our method for extracting velocity tends to underestimate the highest achievable value because we include periods of saltatory motion (Figure 2B) in our calculations.

**Effect of Microtubule Depolymerization.** We previously showed that active transport of PEI/DNA nanocomplexes is microtubule-dependent in that depolymerization of these cytoskeletal structures inhibits active transport, possibly by hindering motor protein-mediated transport along microtubule fibers (10). Figure 4A shows the ensemble-average effective diffusivity curve of gene carriers becomes subdiffusive in nature following microtubule depolymerization. This may be a reflection of the lack of fast-moving actively transported carriers in microtubule-depolymerized cells (Figure 4A). Therefore, to determine how the transport of nonactive gene carriers in nocodazole-treated cells compares to the subpopulation of carriers that are nonactively transported in control cells, the contribution of actively transported carriers was omitted from the overall  $D_{\text{eff}}$  calculations in Figure 4B.

Microtubule depolymerization appears to increase the short-range motion (time scale of 33 ms) of nonactively transported carriers compared to the nonactive carriers in control cells with intact microtubules (Figure 4C). A possible explanation is that depolymerization of microtubules loosens the cagelike microenvironments formed by microtubule fibers, allowing gene carriers greater movement with fewer obstacles. Alternatively, the carriers that are tethered to intact microtubules do not have these attachment sites in cells treated with nocodazole and, therefore, have greater freedom in motion. For either hypothesis, the gene carrier can again be inside or outside of vesicles. The longer range motion (time scale of 3 s) of nonactively transported carriers in nocodazole-treated cells, however, is not statistically different than that of the nonactively transported carriers in cells with intact microtubules (Figure 4C). Long-time diffusion is unaffected by the depolymerization of microtubules, suggesting that other cytoplasmic structures (18) (actin cytoskeleton, ER, etc.) may control the long-range transport of nonactive PEI/DNA nanocomplexes.

### Conclusions

Using real-time live-cell multiple particle tracking, we have begun to uncover the biophysical phenomena underlying the intracellular transport of nonviral gene carriers. We are able to quantify the transport of gene carriers as they traffic within live cells. These studies, as well as others aimed at quantifying particle transport through extracellular barriers to gene delivery (21), may help identify and characterize critical rate-limiting steps to efficient gene delivery and, therefore, should aid in the rational design of more effective carriers.

### Acknowledgment

This work was supported by a Merck Young Investigator Award to J.H., the National Science Foundation (CTS0210718) to D.W., and the National Institutes of Health training grant (T32-GM07057) to J.S.

### References and Notes

- (1) Luo, D.; Saltzman, W. M. Synthetic DNA delivery systems. *Nat. Biotechnol.* **2000**, *18* (1), 33–37.
- (2) Hanes, J.; et al. Gene delivery to the lung. In *Pharmaceutical Inhalation Aerosol Technology*; Hickey, A. J., Ed.; Marcel Dekker Inc.: New York, 2003; pp 489–539.
- (3) Lukacs, G. L.; et al. Size-dependent DNA mobility in cytoplasm and nucleus. *J. Biol. Chem.* **2000**, *275* (3), 1625–1629.
- (4) Pouton, C. W.; Seymour, L. W. Key issues in nonviral gene delivery. *Adv. Drug Deliv. Rev.* **2001**, *46* (1–3), 187–203.
- (5) Kircheis, R.; Wightman, L.; Wagner, E. Design and gene delivery activity of modified polyethylenimines. *Adv. Drug Deliv. Rev.* **2001**, *53* (3), 341–358.
- (6) Remy-Kristensen, A.; et al. Role of endocytosis in the transfection of L929 fibroblasts by polyethylenimine/DNA complexes. *Biochim. Biophys. Acta* **2001**, *1514* (1), 21–32.
- (7) Zabner, J.; et al. Cellular and molecular barriers to gene transfer by a cationic lipid. *J. Biol. Chem.* **1995**, *270* (32), 18997–19007.
- (8) Godbey, W. T.; et al. Poly(ethylenimine)-mediated transfection: a new paradigm for gene delivery. *J. Biomed. Mater. Res.* **2000**, *51* (3), 321–328.
- (9) Gonzalez, H.; Hwang, S. J.; Davis, M. E. New class of polymers for the delivery of macromolecular therapeutics. *Bioconjug. Chem.* **1999**, *10* (6), 1068–1074.
- (10) Suh, J.; Wirtz, D.; Hanes, J. Efficient active transport of gene nanocarriers to the cell nucleus. *Proc. Natl. Acad. Sci. U.S.A.* **2003**, *100* (7), 3878–3882.
- (11) Lee, G. M.; Ishihara, A.; Jacobson, K. A. Direct observation of brownian motion of lipids in a membrane. *Proc. Natl. Acad. Sci. U.S.A.* **1991**, *88* (14), 6274–6278.
- (12) Kusumi, A.; Sako, Y.; Yamamoto, M. Confined lateral diffusion of membrane receptors as studied by single particle tracking (nanovid microscopy). Effects of calcium-induced differentiation in cultured epithelial cells. *Biophys. J.* **1993**, *65* (5), 2021–2040.
- (13) Apgar, J.; et al. Multiple-particle tracking measurements of heterogeneities in solutions of actin filaments and actin bundles. *Biophys. J.* **2000**, *79* (2), 1095–1106.
- (14) Tseng, Y.; Kole, T. P.; Wirtz, D. Micromechanical mapping of live cells by multiple-particle-tracking microrheology. *Biophys. J.* **2002**, *83* (6), 3162–3176.
- (15) Bieber, T.; et al. Intracellular route and transcriptional competence of polyethylenimine-DNA complexes. *J. Controlled Release* **2002**, *82* (2–3), 441–454.
- (16) Fried, J.; Perez, A. G.; Clarkson, B. D. Rapid hypotonic method for flow cytometry of monolayer cell cultures. Some pitfalls in staining and data analysis. *J. Histochem. Cytochem.* **1978**, *26* (11), 921–933.
- (17) Crocker, J. C.; Grier, D. G. U. Methods of digital video microscopy for colloidal studies. *J. Colloid Interface Sci.* **1996**, *179* (1), 298–310.
- (18) Luby-Phelps, K. Cytoarchitecture and physical properties of cytoplasm: Volume, viscosity, diffusion, intracellular surface area. *Int. Rev. Cytol.* **2000**, *192*, 189–221.
- (19) Fujiwara, T.; et al. Phospholipids undergo hop diffusion in compartmentalized cell membrane. *J. Cell Biol.* **2002**, *157* (6), 1071–1081.
- (20) King, S. J.; Schroer, T. A. Dynactin increases the processivity of the cytoplasmic dynein motor. *Nat. Cell Biol.* **2000**, *2* (1), 20–24.
- (21) Dawson, M.; Wirtz, D.; Hanes, J. Enhanced viscoelasticity of human cystic fibrotic sputum correlates with increasing microheterogeneity in particle transport. *J. Biol. Chem.* **2003**, *278* (50), 50393–50401.

Accepted for publication November 14, 2003.

BP034251Y